

Flexible Printed Reference Electrodes for Electrochemical Applications

Libu Manjakkal, Dhayalan Shakthivel, and Ravinder Dahiya*

This work presents screen-printed thick film reference electrodes (REs) on a polyethylene terephthalate substrate. The ion-conducting channel of presented screen-printed thick film Ag|AgCl|KCl electrodes are made from a composite of glass–KCl powder. With this new formulation the REs exhibit negligible variation in the potential (± 4 mV), when evaluated under different bending states (radius 3, 5, and 7 mm). With a stable electrode potential and in-depth electrochemical studies, the utility of the presented REs for pH-sensing and flexible supercapacitor (SC) applications is demonstrated. With amperometric studies, we have shown that for pH-sensing applications, the presented REs can exhibit a sensitivity of $9 \mu\text{A pH}^{-1}$. At 1 mHz, the electrochemical investigations involving presented thick film REs and graphene-based SCs demonstrate a capacitance of $75 \mu\text{F cm}^{-2}$. With a flexible form factor, high endurance, and a miniature size, the presented RE has distinct advantages over conventional glass-based REs, particularly for emerging applications such as flexible sensing and for characterization of materials for energy storage devices.

conventional glass-based REs (GREs) in emerging wearable systems. Besides being nonflexible, the GREs are fragile, and it is difficult to miniaturize and integrate them for multisensor applications.^[4–6] The periodic filling of liquid KCl electrolyte needed in GREs also limits their use in continuous monitoring of health and water quality.^[7,8] These limitations of current REs, along with the huge potential of flexible and wearable systems,^[5,9] are driving the research toward miniaturized and flexible/wearable REs. Currently, there is no commercial RE that could meet the requirements for flexible electrochemical studies.

In terms of the state of the art, various types of REs (Figure 1) have been explored for electrochemical applications. These include standard hydrogen electrode and saturated calomel electrodes ($\text{Hg}|\text{Hg}_2\text{Cl}_2$),^[10]

$\text{Ag}|\text{AgCl}$,^[11,12] and $\text{Cu}|\text{CuSO}_4$.^[13] Among these, the $\text{Ag}|\text{AgCl}$ -based REs are common and more attractive because of easy fabrication, stable electrode potential, and their nontoxicity.^[10,14,15] Conventional REs are fabricated on glass using AgCl coated Ag metal wire in a saturated KCl or enriched Cl^- ion solution.^[8,10,16] However, as discussed earlier, due to rigidity of glass, it is difficult to use GREs in emerging application such as wearables' systems. For this reason, $\text{Ag}|\text{AgCl}$ -based thin^[17,18] and thick film^[19–22] REs have also been explored recently. Although both these types of REs have been shown to have good potential for wearable and disposable devices, they still have several limitations. For example, being a quasi-RE (i.e., absence of KCl layer), the majority of thin film REs exhibit fluctuations in the open circuit potential (OCP) while reacting with Cl^- ions.^[20] The unstable potential due to the decomposition of AgCl layer over a period of time is detrimental to the long-term operation of thin film REs. The absence of KCl in thin film REs also increases the issue of cross-sensitivity^[23] and for this reason thick film RE have been explored. The thick film REs use KCl paste or polymer–KCl composites over AgCl electrode,^[20,21] A common issue with thick films REs is their short lifetime due to rapid decay of KCl layer.^[20,21,24] Further, the polymer-based KCl layer in these REs require long setting-up time (more than 2 h) prior to use. These issues have been overcome in the current work through development of flexible reference electrode (FRE) based on thick film $\text{Ag}|\text{AgCl}|\text{KCl}$.

The thick film $\text{Ag}|\text{AgCl}|\text{KCl}$ -based FRE reported here has been developed with screen printing technique, which is known as a cost-effective electrode fabrication method.^[25,26] The performance of FRE has been evaluated through electrochemical

1. Introduction

Reference electrodes (REs) are key components of fabrication of chemical or biosensors and are central to the electrochemical characterization techniques such as cyclic voltammetry (CV), potentiometry, electrochemical impedance spectroscopy (EIS), etc. They are needed to characterize active working electrode (WE) materials in the energy storage devices such as batteries,^[1] supercapacitors (SCs),^[2] and dye-sensitized solar cell.^[3] REs with stable potential are needed in these cells and in various electrochemical or bio sensing devices (e.g., pH and glucose sensors, etc.) for wearable electronic skin (e-skin) in health monitoring.^[4–6] The electrochemical sensors for wearable systems require REs and sensitive electrodes (SEs) to have flexible form factors. These requirements make it difficult to use

Dr. L. Manjakkal, Dr. D. Shakthivel, Prof. R. Dahiya
Bendable Electronics and Sensing Technologies (BEST) Group
School of Engineering
University of Glasgow
G12 8QQ, Glasgow, UK
E-mail: Ravinder.Dahiya@glasgow.ac.uk

 The ORCID identification number(s) for the author(s) of this article can be found under <https://doi.org/10.1002/admt.201800252>.

© 2018 The Authors. Published by WILEY-VCH Verlag GmbH & Co. KGaA, Weinheim. This is an open access article under the terms of the Creative Commons Attribution License, which permits use, distribution and reproduction in any medium, provided the original work is properly cited.

DOI: 10.1002/admt.201800252

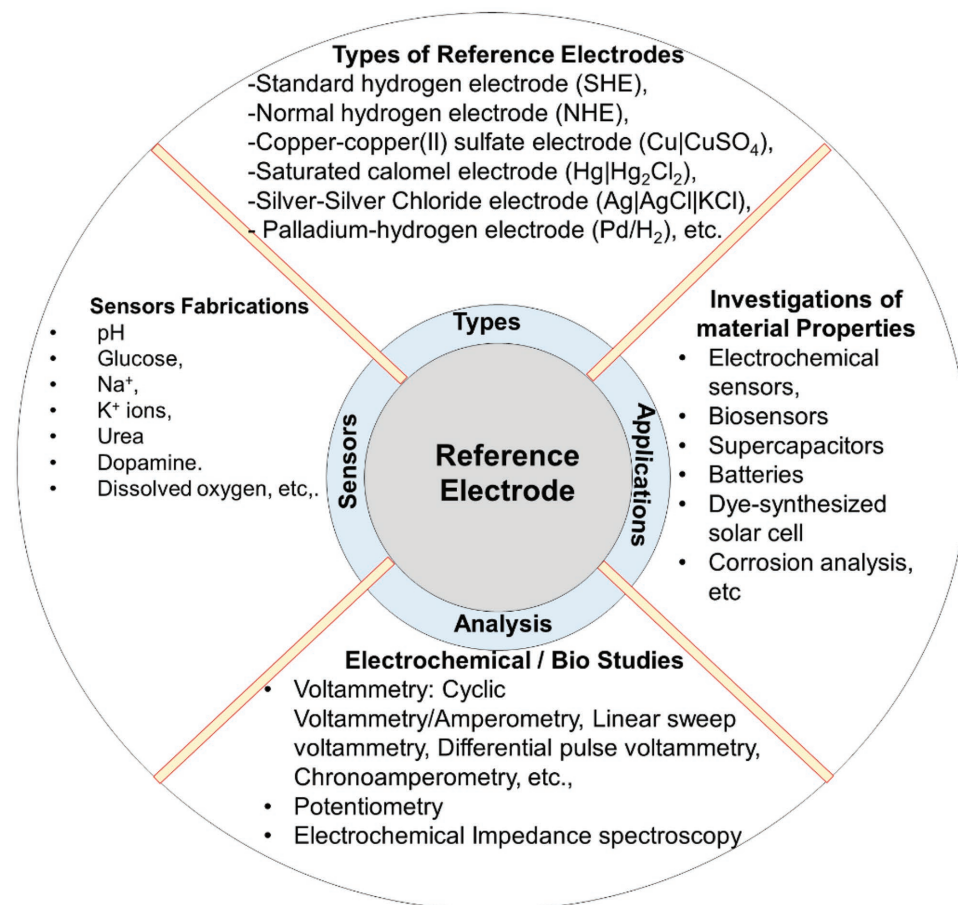


Figure 1. Distinct types of RE (top) and its applications in sensors fabrication (right), investigation of material property of different devices (left) using different analysis method (bottom).

studies involving: a) evaluation of electrode potential, b) pH sensor characterization, and c) characterization of active electrode of SCs. The FREs were implemented to test the electrochemical performance of RuO₂-based pH sensor in different buffer solutions and also with graphene-based SC. Currently, majority of the electrochemical studies related to SC/batteries use an external GRE. Our electrochemical studies reveal that the FRE will be attractive alternative to GREs for the investigations related to the performance evaluation of active electrode material of SCs in a three-electrode system.

2. Results and Discussion

2.1. Structural Characterization

The surface morphology and cross-sectional view of the Ag and glass-KCl layers were imaged using scanning electron microscopy (SEM) as shown in the images in **Figure 2**. Figure 2a shows the surface morphology of conducting Ag electrode on polyethylene terephthalate (PET) substrate. The screen printing used here is a promising method as the electrode shows continuous, dense, and porous structure. After chloridization of Ag electrode layer, the glass-KCl layer was printed on it and the surface

morphology is shown in Figure 2b. The surface morphology of the glass-KCl film shows porous microcrystalline structure with the size in the range of few microns. The printing process also ensured that the glass-KCl composite paste was strongly adhered on to the AgCl layer and PET. The tilted view of the composite film with PET (Figure 2c) shows the structural uniformity across the cross section. The approximate thickness of the film observed from the cross-sectional view is around 12 μm. The high-resolution image (Figure 2d) of KCl composite shows the resulted porous morphology and the micron sized (0.5–0.8 μm) crystalline structure crystals. The cross-sectional image in Figure 2e shows that the KCl composite film prepared using copolymer and KCl powder is strongly adherent to the Ag electrode film. This strong adhesion allows the RE to withstand the bending stress. The SEM image shown in Figure 2e, after pH measurement, reveals an excellent stability. The pore size (surface area) of the film was measured from SEM image (Figure 2b) by using ImageJ software. The analysis showed that the average pore size distribution of electrodes is about 22 nm (Figure 2f). The macroscopic roughness and porosity of the film lead to faster responsivity of the electrodes.^[27] The roughness and porosity strongly influence the electrode-solution interaction and lead to improved electrochemical performance. To investigate the electrode-electrolyte interaction, we also

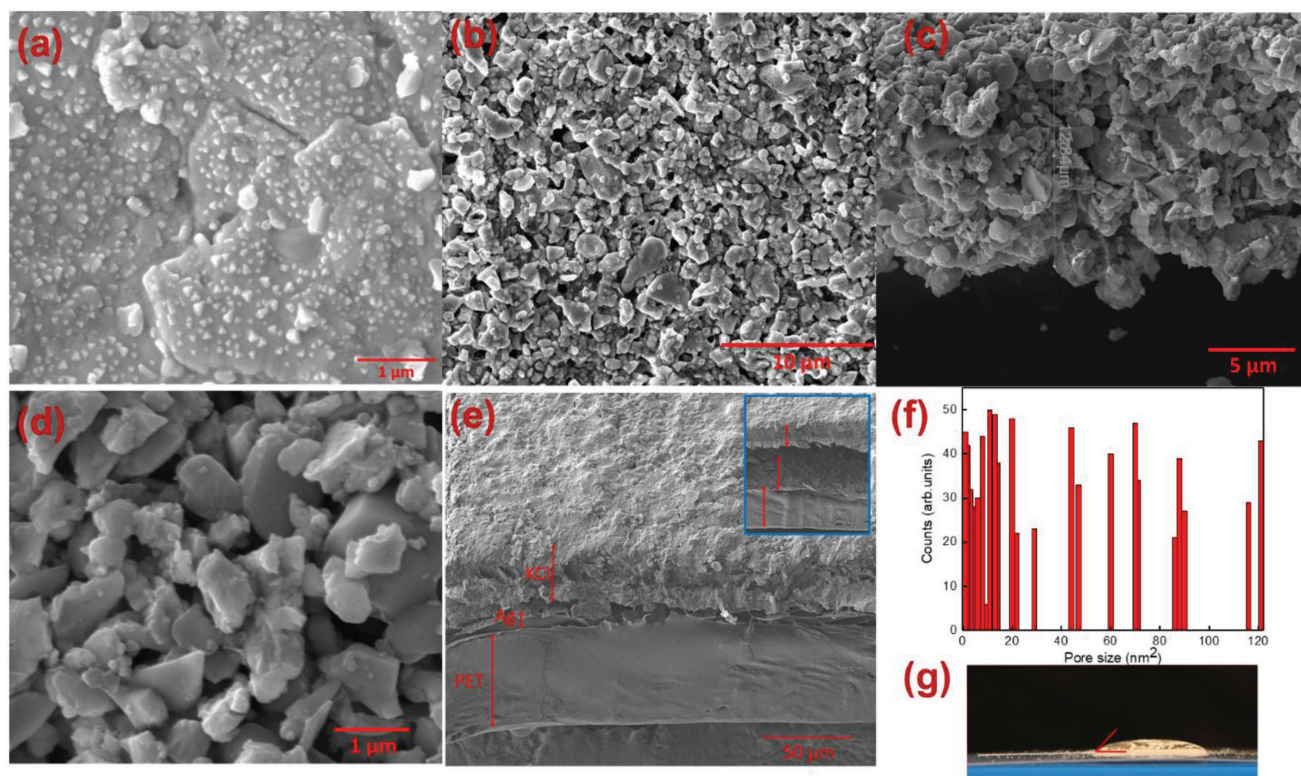


Figure 2. SEM image of a) surface morphology of Ag electrode over PET, b) top view of glass–KCl composite film, c) tilted view of glass–KCl composite film, d) glass–KCl composite on the top of AgCl layer, e) cross-sectional view shows various layers of the FRE film, f) pore size distribution measured from post-processing of SEM image using ImageJ software tool, and g) optical image of contact angle measurement.

measured the contact angle by using an optical image of FRE film in contact with de-ionized water, as shown in Figure 2g. The observed contact angle is about 48°, which indicates the hydrophilic nature of film while reacting with the solution. This strong interaction of FRE with the solution enhances the performance of sensors.

2.2. Evaluation of Electrode Potential

A stable potential is required for the use of the REs in any sensor or other electrochemical characterizations. Figure 3a shows the variation of OCP of FRE against a commercial GRE in buffer solution of pH value 7. When a thick film RE is dipped in the test solution, the ions in solution are transported through the hydration port and reach the electrode surface. This process creates a potential difference with respect to other electrodes which are used for testing. From the OCP of FRE versus GRE, we found that during initial measurement the value of OCP was unstable and showed weak signal due to the hydration response of the glass KCl composite film. After initial stabilization phase of about 2 h, the potential became stable with the magnitude of 68 mV. It was found that the ion conductive KCl channel of the newly printed electrodes functions properly because of the initial stabilization phase. However, the glass–KCl composite used ethyl cellulose as a binder for the paste formation, which has lower value of the potential against GRE (≈ 10 mV).^[11,28] Currently, we have used a

copolymer-based binder paste. Generally, the binder materials are known to influence the hydration time and stability.^[20,21] After initial stabilization phase, both the FRE and RRE were found to stabilize to their OCP values in less than 20 min (after storing the electrode in the dry atmosphere). The glass–KCl composite based REs stabilize faster than the polymer–KCl matrix based thick film REs. This is due to the high mobility of the Cl^- ion in the case of glass–KCl paste with respect to polymer-based KCl paste.^[20,21]

The comparison of OCP of GRE and FRE with RuO_2 -based SE is also presented in Figure 3a. The performance of thick film RE was evaluated by measurement of OCP against and pH SE. The comparisons of OCPs of GRE and FRE with SE (shown in plots (ii) and (iii), respectively) are given in Figure 3a. It may be observed that the SE shows a potential of 30 mV against GRE and -31 mV against FRE. This difference is because of stable potential value of FRE, as observed in the curve (i) of Figure 3a. Hence, thick film FRE shows stable potential when used for pH-sensing application. A further analysis is given in the following section.

For flexible electronics applications, the evaluation of the values of OCP under different bending conditions is crucial. Figure 3b shows the OCP values of FRE against GRE under bending radii of 3, 5, and 7 mm. The bending appears to have little influence of the OCP values as the variation with bending is low (± 4 mV). While implementing the FREs for sensors applications, this observed variation in the value of OCP could be easily compensated with electronics.

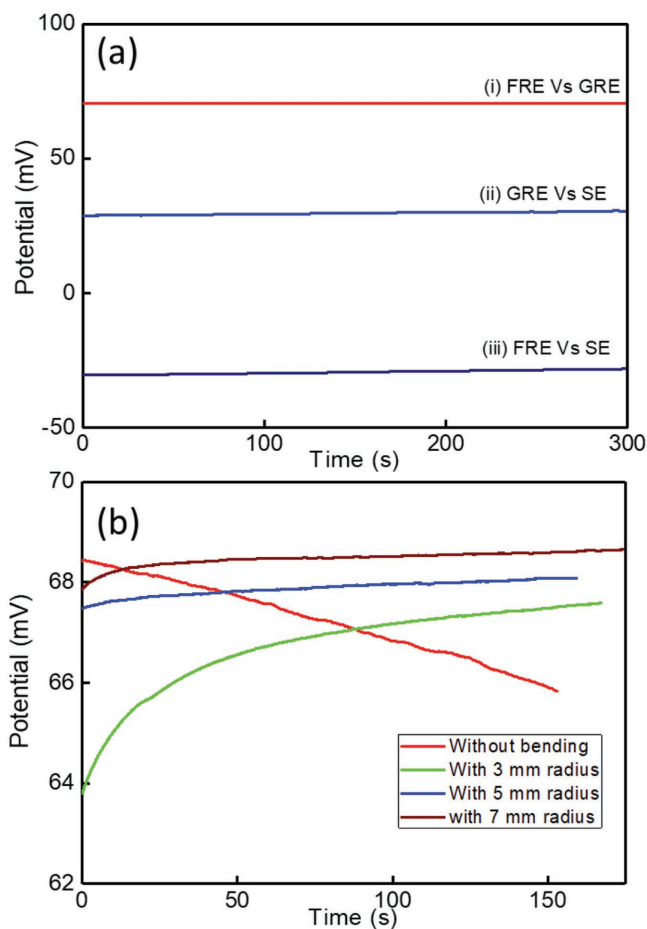


Figure 3. a) The OCP between the i) FRE versus GRE, ii) GRE versus SE, iii) FRE versus SE and b) the potential variation with and without bending of FRE.

2.3. Amperometric pH Sensor Characterization

A further analysis of REs for pH-sensing application was carried (with SEs from $\text{RuO}_2\text{-Ta}_2\text{O}_5$) through CV analysis in varied pH solutions, as shown in Figure 4. Figure 4a show the CV plots of SE with FRE from this work. The plots were obtained for a pH range of 4–10 at a sweep rate of 100 mV s^{-1} . The observed redox peaks in the CV spectrum is due to the influence of redox reaction of active RuO_2 -based SE electrode. In the pH range 4–8, we have observed a variation of $\approx 9 \mu\text{A pH}^{-1}$ at 1 V. For pH 8 solution, the comparison of FRE (Figure 4b) with GRE and RRE in the CV spectrum shows that that redox peaks are almost similar with minor shift in peak position and height. The variation in the peak position in GRE, RRE, and FRE against RE could be due to the influence of potential and the flow of current in thick film electrode. As compared with GRE, the FRE current flow is higher in redox reactions due to low impedance and is observed in the EIS analysis. The CV analysis demonstrated that the presented FREs are suitable for amperometric analytical measurements for characterization of sensors.

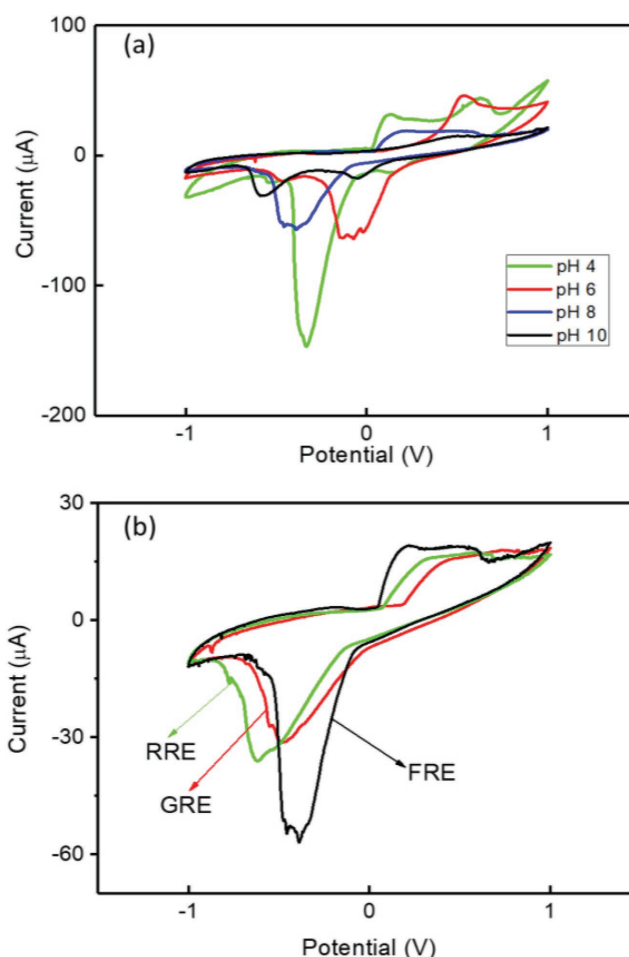


Figure 4. a) CV spectrum of thick film pH SE with FREs in pH buffer solutions and b) comparison of GRE, RRE and FRE with SE at pH 8 buffer.

2.4. Thick Film Reference Electrodes for Characterization of Energy Storage Devices

For SC and battery applications, it is important to evaluate the electrochemical performance with CV and EIS analysis, etc.^[29–31] to predict the performance of devices. Figure 5a shows the comparison of CV analysis of two-electrode system (WE vs GRE and WE vs FRE) at 100 mV s^{-1} sweep over H_3PO_4 electrolyte. The CV analysis reveals that the shape of the spectra are apparently same, with minor variation in peak maxima and area of the curve. The large cathodic peak is observed for WE versus FRE in Figure 5a is similar those observed for pH sensor applications. This is attributed to the working potential window of SC. Due to non-Faradaic reaction of the multilayered graphene sheet (MGS) in aqueous electrolyte, there is no redox reaction observed in the CV spectrum.^[32] In addition to this, we observed that the FRE can be used to operate at a wide scan rate ($50\text{--}300 \text{ mV s}^{-1}$; Figure 5b). It was observed that with increase in the scan rate from 50 to 300 mV s^{-1} , the increased in the peak current is similar to the reported works on SC characterization with external GRE.^[29] A similar observation was found with NaCl electrolytes.

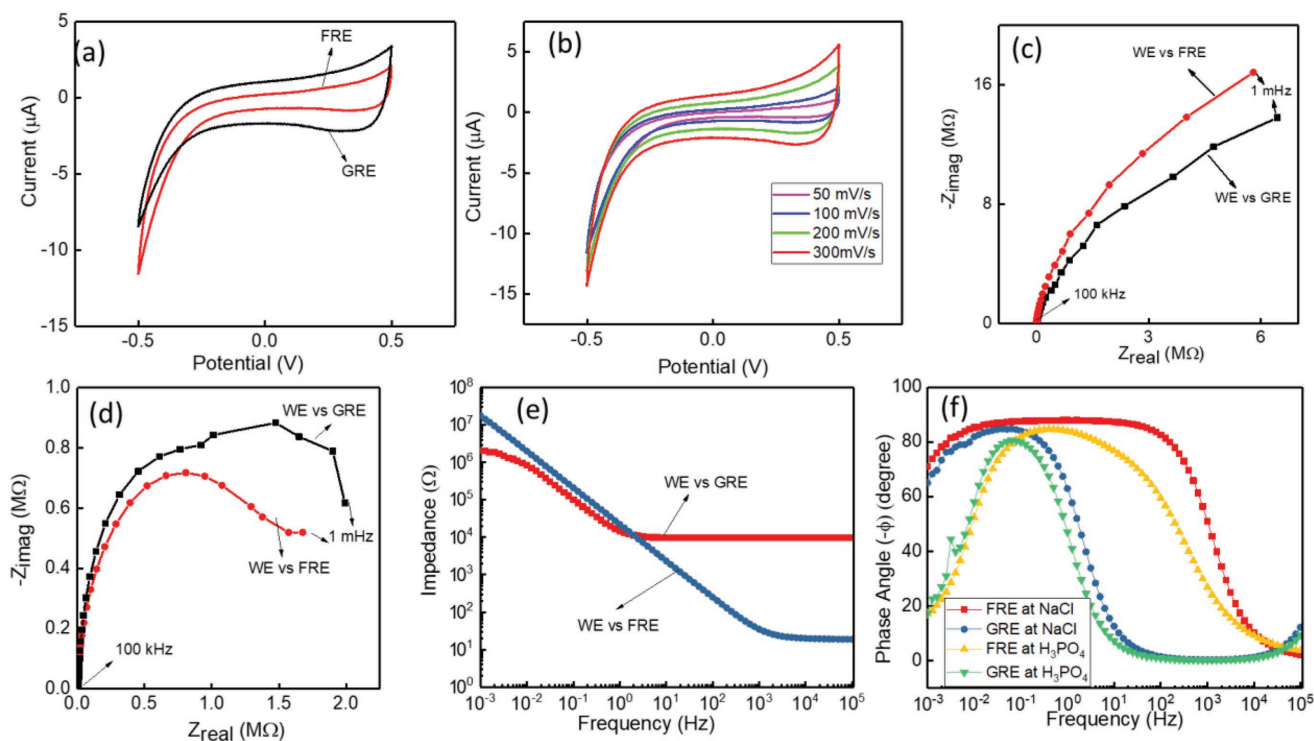


Figure 5. Electrochemical analysis of graphene electrode for SCs in two-electrode system a) comparison of CV analysis of WE with GRE and WE with FRE in H_3PO_4 electrolyte. b) CV spectra of WE with FRE at different scan rates. c,d) Comparison of Nyquist plot of WE with GRE and WE with FRE at H_3PO_4 and NaCl electrolyte, respectively. e) Bode impedance plot for WE versus FRE and WE versus GRE in H_3PO_4 electrolyte, and f) comparison of Bode plots for WE with GRE and FRE for NaCl and H_3PO_4 electrolytes.

The capacitive performance of WE and the ion exchange reaction between the WE–electrolytes (i.e., 3 M NaCl and H_3PO_4) interface were investigated by using EIS analysis (Figure 5c–f) in two-electrode systems. The observed Nyquist plots from complex impedance data for the WE versus GRE and FRE in H_3PO_4 and NaCl solutions is shown in Figure 5c,d respectively. From the Nyquist plots, it is observed that the variation in magnitude of real and imaginary parts of the impedance is similar. Even though the electrolyte and WE are similar, a significant difference in real part of impedance (Z_{real}) was observed in the high-frequency range, as shown in Figure 5e for H_3PO_4 . This difference in impedance in the high-frequency range is due to the influence of REs. In comparison with FREs, the impedance value of GRE at high frequency (100 kHz) is almost 500 times higher. Generally, Z_{real} at higher frequencies is due to the charge transfer resistance of electrode material, and resistance due to electrode–electrolyte interaction.

The Bode phase plot of EIS analysis shown in Figure 5f confirms the influence of frequency on the electrodes performance. Figure 5f compares the Bode angle plot for GRE- and FRE-based measurements in both NaCl and H_3PO_4 electrolytes. The characteristic frequency (f_0), the frequency at -45° phase angle where the capacitive and resistive impedances are equal, of the device in different electrolytes can be obtained from Figure 5f. With f_0 of the SC, the relaxation time constant (τ_0) can be obtained using:

$$\tau_0 = 1/f_0 \quad (1)$$

The comparison of f_0 and τ_0 for measurement of FRE and GRE with MGS for NaCl and H_3PO_4 for two-electrode systems is shown in Table 1. For both electrolytes the value of f_0 is higher in FRE (in two-electrode system) and the corresponding τ_0 for MGS electrode is in the range of milliseconds. This variation in frequency and time constant could be due to the low impedance of electrode while reacting with solution. Hence, EIS analysis of two-electrode system measurement shows that there is current flow in thick film RE, which influences the charge transfer resistance of the electrode and hence the measurements.

A further analysis of the influence of electrode configuration on EIS analysis was carried out by using a three-electrode system. Figure 6a shows the variation of impedance with frequencies for WE against GRE, RRE, and FRE in NaCl electrolyte solution. It may be noted from Figure 6a that the impedance in high-frequency range is almost the same. This is dissimilar to the measurements in a two-electrode system (Figure 5) where significant difference was observed in the

Table 1. Comparison of characteristic frequency and relaxation time for SC electrode measurement with GRE and FRE.

Parameter	NaCl		H_3PO_4	
	GRE	FRE	GRE	FRE
f_0 [Hz]	2.1	1262	1.12	298
τ_0 [s]	0.47	0.7×10^{-3}	0.89	3.3×10^{-3}

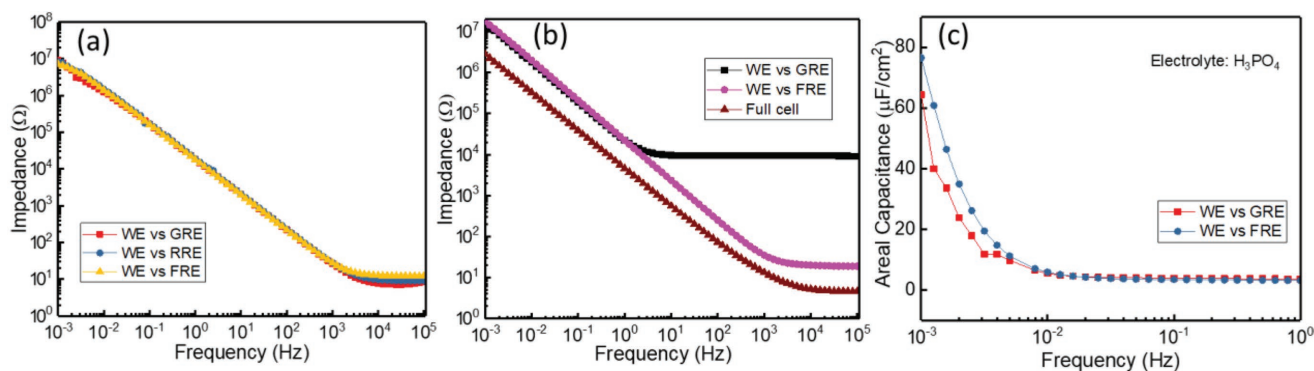


Figure 6. The EIS analysis of a) three-electrode system, b) two-electrode systems with full cell, and c) areal capacitance variation with frequency.

high-frequency range. Hence, the electrode configuration for measurement influences the EIS analysis. To investigate the full cell for symmetric SC^[2,30] with the two-electrode configuration, we carried out the EIS analysis and measured impedance variation to compare with the analysis made with presented FRE and GRE. Figure 6b shows the comparison of impedance changes in NaCl electrolyte. It shows that the passage of current in thick film RE, the FRE, and full cell demonstrates similar electrochemical performance.

We have obtained the areal capacitance (C_A) of SC by using the following expression.

$$C_A = -1/(2\pi f Z_{\text{imag}}) \quad (2)$$

where f is the frequency and Z_{imag} is the imaginary part of the complex impedance. The variation in C_A with f is shown in Figure 6c. In low-frequency range, the areal capacitance for both FRE- and GRE-based measurements is in the order of tens of $\mu\text{F cm}^{-2}$ for H_3PO_4 electrolyte which is similar to that of symmetric full cell of SC. Comparison of C_A for MGS with different electrodes and measurements is given in Table 2. Here we found that at 1 mHz, the SC has capacitance of $75 \mu\text{F cm}^{-2}$ for WE versus FRE and $65 \mu\text{F cm}^{-2}$ for WE versus GRE. This difference in capacitance is due to different ionic resistances offered by the electrodes as a result of varied diffusion of ions at low frequencies (Figure 5c). In the EIS measurement, the WE versus FRE shows a lower value of resistance than for WE versus GRE. When we compare the value of C_A of SC for NaCl and H_3PO_4 electrolytes, the H_3PO_4 -based devices show higher value of areal capacitance. This is because of higher mobility of H^+ , in comparison to Na^+ , and matches with previous reports.^[32] From these analysis, we can confirm that for three-electrode system measurements related to energy storage material for SC and batteries, the thick film REs offer an attractive alternative for the bulky GREs.

Table 2. Comparison of the capacitance of SC in H_3PO_4 solution for two-electrode system.

Cell configuration	Capacitance [$\mu\text{F cm}^{-2}$]
WE versus GRE	65
WE versus FRE	75
Full cell	59

3. Conclusion

The presented flexible Ag|AgCl|KCl-based thick film REs on flexible PET substrates, with stable OCP, offer an attractive alternative for the bulky GREs. The stable OCP (68 mV vs glass-based Ag|AgCl RE) of FREs is owing to the new glass-KCl composite based paste, which is screen printed on to AgCl layer. Further, the presented FRE exhibits negligible variation (± 4 mV) in OCP with different bending conditions. The fabricated FREs have been evaluated against GRE, in context with their suitability for characterizing electrochemical pH sensors and the electrodes of SCs. The amperometric pH sensing shows that the FREs with RuO_2 -based pH-sensing electrode exhibits a sensitivity of $9 \mu\text{A pH}^{-1}$. The electrochemical investigation of FRE with graphene electrode for SCs with H_3PO_4 electrolyte shows a capacitance of $75 \mu\text{F cm}^{-2}$ at 1 mHz. These results show that the fabricated thick film FREs can be implemented for wearable sensors and for electrochemical characterization of active electrode material for several applications.

4. Experimental Section

Screen printing technique was used in this work to fabricate the thick film FREs. Initially, for making the a glass powder-KCl composite paste, the KCl powder was prepared by milling the KCl salt in isopropyl alcohol (IPA) with a planetary ball mill for 2 h. After milling step, the slurry was transferred to a petri dish and this was annealed at 80°C for 2 h to remove the IPA content. The resulting fine KCl powder was mixed in equal weight (1:1) proportion with a lead free glass powder composite in presence of IPA. This was followed by ball milling for 3 h to obtain a homogeneous mix of glass-KCl composite. The mixture was dried at 80°C for 2 h. To prepare the paste suitable for printing, the glass-KCl composite powder for 30 min in an agate mortar was thoroughly mixed with a binder made of copolymer of poly (methyl methacrylate), poly (butyl methacrylate), and using butyl carbitol acetate as solvent. This binder was cured at $\approx 120^\circ\text{C}$, which is suitable for fabrication of flexible electrodes.^[26]

The fabrication steps of the proposed FRE are shown in Figure 7a. As a first step, the Ag paste (DuPont 5000) was printed on PET substrate, followed by annealing at 120°C for 1 h. With this a strongly conductive flexible Ag electrode was obtained. Initially, one end of the Ag electrode was converted into AgCl layer by chloridization during dip coating.^[11,33] The Ag electrode end was dipped for 1 min in sodium hypochlorite solution (Sigma-Aldrich). Further, the glass-KCl composite paste was screen printed on AgCl layer and dried at 120°C for 2 h. The glass-KCl layer served as the salt bridge in solid-state thick film RE. To reduce the decay time of glass-KCl layer (while reacting with the test solution), a

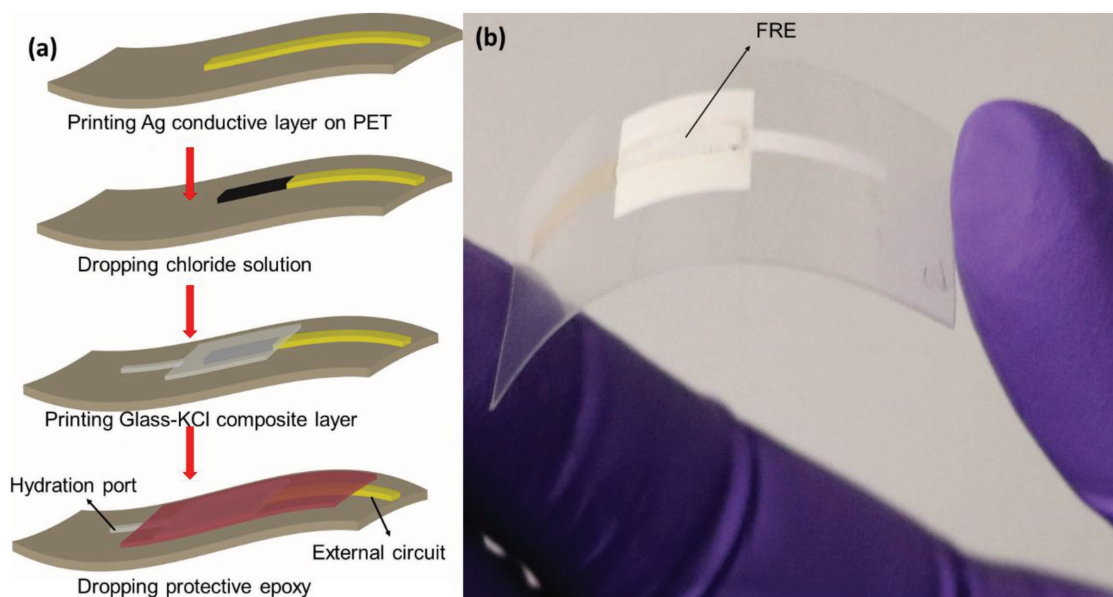


Figure 7. a) Fabrication steps of FRE and b) image of FRE.

polyurethane resin based insulating epoxy layer was coated on to the electrode.^[24] Polyurethane offered flexibility and protected the RE from rapid decay of KCl. While coating the protective resin, a small slit for the hydration port was left to allow the penetration of solution to electrode, as shown in Figure 7a. The other end of Ag electrode was used for external circuit connection. The image of fabricated FRE is shown in Figure 7b.

The surface morphology of thick film glass–KCl composite was observed with scanning electron microscopy (FEI Nova NanoSEM) and the electrochemical measurements were carried out for two- and three-electrode systems with Metrohm Autolab (PGSTAT302N, Netherland). For testing the performance of FRE, commercial GRE (Sigma Aldrich, UK) thick film rigid RE (RRE)^[28] fabricated on alumina substrate and RuO₂-based pH-sensing electrode were used.^[22] The FRE was characterized to measure their OCP response against a commercial GRE (Autolab, Netherland) and RuO₂-based pH SE in a buffer solution of pH value 7. The influence of bending on OCP of the FRE was evaluated by bending them (over radius of curvatures of 3, 5, and 7 mm). The sensing performance of the developed FRE was demonstrated by using pH-sensing electrode. The analytical performance of the sensor was monitored with CV analysis of FREs against the sensing electrode. Here CV analysis of the pH SE was carried out against GRE, RRE and FRE in pH buffer solution in the range of 4–10.

To investigate the electrochemical performance of SCs based on MGS (Graphene Supermarket, US), CV and EIS analysis for two and three-electrode systems were performed. In three-electrode system, Pt was used as a counter electrode, and the proposed RE and MGS were used as WE. For a two-electrode system, the FRE served as shared counter and RE. The electrochemical performance of the WE were also compared with GRE and FRE/RRE. The CV analysis was carried out by varying the scan rate from 5 to 300 mV s⁻¹ between +0.5 and –0.5 V. The EIS analysis was carried out at frequency range of 1 mHz to 100 kHz with 10 mV sinusoidal signal. The 3 m NaCl and H₃PO₄ solutions were used for electrochemical study of SC electrolytes. The SC performance was evaluated by developing a full cell using two identical MGS electrodes and cellulose/polyester as a separator.

Acknowledgements

This work was partially supported by EPSRC Engineering Fellowship for Growth under Grant No (EP/M002527/1). The authors are thankful to

the support received for this work from James Watt Nanofabrication Centre (JWNC) University of Glasgow, U.K.

Conflict of Interest

The authors declare no conflict of interest.

Keywords

Ag|AgCl|KCl electrodes, electrochemical study, flexible reference electrode, pH sensor, screen printing

Received: July 8, 2018

Revised: August 21, 2018

Published online: September 21, 2018

- [1] J. Landesfeind, D. Pritzl, H. A. Gasteiger, *J. Electrochem. Soc.* **2017**, *164*, 1773.
- [2] S. Zhang, N. Pan, *Adv. Energy Mater.* **2015**, *5*, 1401401.
- [3] J. Wu, Y. Li, Q. Tang, G. Yue, J. Lin, M. Huang, L. Meng, *Sci. Rep.* **2014**, *4*, 4028.
- [4] T. Guinovart, G. Valdés-Ramírez, J. R. Windmiller, F. J. Andrade, J. Wang, *Electroanalysis* **2014**, *26*, 1345.
- [5] W. Dang, L. Manjakkal, W. T. Navaraj, L. Lorenzelli, V. Vinciguerra, R. Dahiya, *Biosens. Bioelectron.* **2018**, *107*, 192.
- [6] W. Gao, S. Emaminejad, H. Y. Y. Nyein, S. Challa, K. Chen, A. Peck, H. M. Fahad, H. Ota, H. Shiraki, D. Kiriya, D.-H. Lien, G. A. Brooks, R. W. Davis, A. Javey, *Nature* **2016**, *529*, 509.
- [7] S. Zhuiykov, *Sens. Actuators, B* **2012**, *161*, 1.
- [8] P. Kurzweil, *Sensors* **2009**, *9*, 4955.
- [9] C. G. Núñez, W. T. Navaraj, E. O. Polat, R. Dahiya, *Adv. Funct. Mater.* **2017**, *27*, 1606287.
- [10] M. W. Shinwari, D. Zhitomirsky, I. A. Deen, P. R. Selvaganapathy, M. J. Deen, D. Landheer, *Sensors* **2010**, *10*, 1679.
- [11] L. Manjakkal, K. Cvejic, J. Kulawik, K. Zaraska, D. Szwagierczak, R. P. Socha, *Sens. Actuators, B* **2014**, *204*, 57.

- [12] Ł. Tymecki, E. Zwierkowski, R. Koncki, *Anal. Chim. Acta* **2004**, 526, 3.
- [13] F. Scholz, *Electroanalytical Methods*, Springer, Berlin, Heidelberg **2010**.
- [14] J. Fernandes, E. Heinke, *J. Sens. Sens. Syst.* **2015**, 4, 53.
- [15] E. T. S. G. da Silva, S. Miserere, L. T. Kubota, A. Merkoçi, *Anal. Chem.* **2014**, 86, 10531.
- [16] W. Vonau, W. Oelßner, U. Guth, J. Henze, *Sens. Actuators, B* **2010**, 144, 368.
- [17] T. Y. Kim, S. A. Hong, S. Yang, *Sensors* **2015**, 15, 6469.
- [18] Q. Li, W. Tang, Y. Su, Y. Huang, S. Peng, B. Zhuo, S. Qiu, L. Ding, Y. Li, X. Guo, *IEEE Electron Device Lett.* **2017**, 38, 1469.
- [19] I. Shitanda, M. Komoda, Y. Hoshi, M. Itagaki, *Analyst* **2015**, 140, 6481.
- [20] M. Sophocleous, J. K. Atkinson, *Sens. Actuators, A* **2017**, 267, 106.
- [21] A. W. J. Cranny, J. K. Atkinson, *Meas. Sci. Technol.* **1998**, 9, 1557.
- [22] L. Manjakkal, K. Zaraska, K. Cvejic, J. Kulawik, D. Szwagierczak, *Talanta* **2016**, 147, 233.
- [23] S. Huang, Y. Jin, Z. Su, Q. Jin, J. Zhao, *Anal. Methods* **2017**, 9, 1650.
- [24] B. J. Polk, A. Stelzenmuller, G. Mijares, W. MacCrehan, M. Gaitan, *Sens. Actuators, B* **2006**, 114, 239.
- [25] M. Simić, L. Manjakkal, K. Zaraska, G. M. Stojanović, R. Dahiya, *IEEE Sens. J.* **2017**, 17, 248.
- [26] L. Manjakkal, B. Sakthivel, N. Gopalakrishnan, R. Dahiya, *Sens. Actuators, B* **2018**, 263, 50.
- [27] W. P. Ouajai, P. J. Pigram, A. Sirivat, *Int. J. Appl. Sci. Technol.* **2016**, 9, 225.
- [28] L. Manjakkal, A. Vilouras, R. Dahiya, *IEEE Sens. J.* **2018** 1–1 (<https://doi.org/10.1109/JSEN.2018.2840349>).
- [29] J. Jjiang, Y. Li, J. Liu, X. Huang, C. Yuan, W. Lou Xiong, *Adv. Mater.* **2012**, 24, 5166.
- [30] Z. Wu, L. Li, J. M. Yan, X. b. Zhang, *Adv. Sci.* **2017**, 4, 1600382.
- [31] L. Manjakkal, C. G. Núñez, W. Dang, R. Dahiya, *Nano Energy* **2018**, 51, 604.
- [32] Q. Chen, X. Li, X. Zang, Y. Cao, Y. He, P. Li, K. Wang, J. Wei, D. Wu, H. Zhu, *RSC Adv.* **2014**, 4, 36253.
- [33] B. E. Horton, S. Schweitzer, A. J. DeRouin, K. G. Ong, *IEEE Sens. J.* **2011**, 11, 1061.